HTD-Vol. 196

G. S. DULIKRAVICH

TRANSPORT PHENOMENA IN MATERIALS PROCESSING AND MANUFACTURING

presented at
THE 28TH NATIONAL HEAT TRANSFER CONFERENCE
AND EXHIBITION
SAN DIEGO, CALIFORNIA
AUGUST 9–12, 1992

sponsored by
THE HEAT TRANSFER DIVISION, ASME

edited by
M. CHARMCHI
UNIVERSITY OF MASSACHUSETTS

S. M. WALSH
U.S. ARMY MATERIALS LAB

K. M. MOALLEMI
POLYTECHNIC UNIVERSITY

M. CHEN
NATIONAL SCIENCE FOUNDATION

F. INCROPERA
PURDUE UNIVERSITY

T. BERGMAN
UNIVERSITY OF TEXAS, AUSTIN

Y. JOSHI
NAVAL POSTGRADUATE SCHOOL

R. L. MAHAJAN
UNIVERSITY OF COLORADO

THE AMERICAN SOCIETY OF MECHANICAL ENGINEERS
United Engineering Center • 345 East 47th Street • New York, N.Y. 10017

HTD-Vol. 196, Transport Phenomena in Materials
Processing and Manufacturing
ASME 1992

MAGNETIZED FIBER ORIENTATION CONTROL IN SOLIDIFYING COMPOSITES: NUMERICAL SIMULATION

George S. Dulikravich and Branko Kosovic
Department of Aerospace Engineering
Pennsylvania State University
University Park, Pennsylvania

ABSTRACT

This work deals with the development of a numerical algorithm for the prediction of magnetic force lines inside a flowing solidifying melt with the ultimate purpose of simulating and controlling alignment of short nickel coated fibers during the curing process in composites. A complete mathematical model and an accompanying computer program have been developed for the computational simulation of a steady laminar flow of an incompressible fluid with strong heat transfer (involving solidification) and a strong superimposed magnetic field. An extended form of the Boussinesq approximation allowing for temperature-dependent physical properties of the fluid including latent heat of phase change was incorporated. This formulation simultaneously predicts detailed velocity, pressure and temperature fields for the moving fluid while capturing the forming solid phase by using a single computer code. The same code can simulate the reverse process of thawing or melting of the solid phase. The computed example configurations involve a two-dimensional closed container, a straight and a U-shaped channel, and a passage of an arbitrary shape. It was found that the presence of an external steady magnetic field: a) diminishes flow field vorticity, b) causes higher velocity gradients within the boundary layers, c) inhibits the solid phase accretion rate and the total amount of solid accrued, and d) is able to orient magnetized fibers along the lines of local magnetic forces.

NOMENCLATURE

c_p = specific heat at constant pressure, J kg^{-1} K^{-1}
c_v = specific heat at constant volume, J kg^{-1} K^{-1}
E = electric field, V m^{-1}
Ec = Eckert number
Fr = Froude number
g = gravity force per unit volume, m s^{-2}
Gr = Grashof number
H = magnetic field, H kg^{-1}
Ht = Hartmann number
J = electric current density, A m^{-2}
k = heat conductivity coefficient, W m^{-1} K^{-1}
l = length, m
L = latent heat of liquid/solid phase change, J kg^{-1}
M_m = magnetic Mach number ($M_m^2 = R_e R_m / Ht^2$)
p = pressure, kg m^{-1} s^{-2}
P_m = magnetic Prandtl number
P_r = Prandtl number
R_e = hydrodynamic Reynolds number
R_m = RePm = magnetic Reynolds number
S = volume fraction of the liquid phase
t = time, s
T = absolute temperature, K
$\Delta T_o = T_h - T_c$ = temperature difference, K
v = (u,v,w) = velocity vector, m s^{-1}
x,y,z = cartesian coordinates, m
α = thermal expansion coefficient, K^{-1}
β = artificial compressibility coefficient
θ = nondimensional temperature
ρ = density, kg m^{-3}
η = coefficient of shear viscosity, kg m^{-1} s^{-1}
ζ = coefficient of secondary viscosity, kg m^{-1} s^{-1}
ξ, η, ζ = non-orthogonal grid-following coordinates
μ = magnetic permeability, H m^{-1}
σ = electrical conductivity, Ω^{-1} m^{-1}
ϕ = nondimensional gravity potential
Φ = viscous dissipation function, kg m^{-1} s^{-3}

subscripts

c = cold wall
h = hot wall
o = reference values
sol = solidus
liq = liquidus

superscripts

* = nondimensional values
' = function of nondimensional temperature

INTRODUCTION

It is well known that the defects in short fiber composites that are mainly due to uncontrolled fiber orientation during composites manufacturing can reduce the strength of the composite (Cranston and Reitz, 1980; Hatta and Yamashita, 1988). Thus, it would be very desirable to perform a solidification of the resin where the local concentration and orientation of the fibers is fully controlled. The objective of this paper is to elaborate on a mathematical model and an accompanying numerical algorithm that are capable of simulating fully three-dimensional ferromagnetic fluid flow (representing the resin and the suspended nickel coated fibers) and solidification under the influence of an arbitrarily distributed and oriented external magnetic field. The basic idea is that the coated fibers will align with the local magnetic lines of force. The pattern of these lines depends on the flow field and the variation of the externaly applied magnetic field.

During a controlled solidification process (Dulikravich and Hayes, 1988), it is very important to fully understand the process of solid phase formation. The accumulated solid phase effectively reduces and deforms the cross sectional area of the passages and causes significant local variations in pressure and flow field shear stresses. During the solidification or melting process, secondary flows are generated due to strong thermal buoyancy forces. These processes cannot be effectively controlled in the case of strong heat transfer, except if influenced by a global body force.

One such body force is the general electromagnetic Lorentz force which is created in any electrically conducting fluid when either a magnetic field or an electric potential field is applied. It has been shown (Lee and Dulikravich, 1991a; Lee and Dulikravich, 1991b; Lee, Dulikravich and Kosovic, 1991a; Dulikravich, Kosovic and Lee, 1991a; 1991b; Kosovic, Dulikravic and Lee, 1991; Dulikravich and Kosovic, 1992) that the magnetic field can eliminate vorticity from the flow field, while the electric field can enhance it (Lee, Dulikravich and Kosovic, 1991b). During the curing process in composites manufacturing, we usually work with electrically conducting resins. They are conducting either because of the presence of iron atoms, salts, or acids. Nevertheless, if fibers are coated with a thin layer of a ferromagnetic material, the fibers will respond to the applied electromagnetic fields by rotating and translating so that they become aligned with the magnetic lines of force (Hatta and Yamashita, 1988; Yamashita et al, 1989; Gandhi, Thompson and Choi, 1989). This is especially true for short fibers (Hatta and Yamashita, 1988). Thus, if a relatively strong magnetic field is applied, the flow field will respond (Heiser, 1964; Ievlev and Levy, 1989; Ozoe and Okada, 1989) and the solid/liquid front shape and speed could be manipulated (Vives, 1989; Dulikravich, Kosovic and Lee, 1991b; Dulikravich and Kosovic, 1992). In this work we have formulated the entire problem as time-dependent and three-dimensional although our computational results will be for steady two-dimensional situations only.

ANALYTICAL MODEL

From Maxwell's equations and a relationship between an induced electric current, J_i, an electric field, E_i, and an externally applied magnetic field, H_i, in a moving media given by Ohm's law

$$J_i = \sigma \left(E_i + \mu \, \varepsilon_{ijk} v_j H_k \right) \tag{1}$$

where σ, μ, and v_j are the coefficient of electric conductivity, coefficient of magnetic permeability, and fluid velocity vector, respectively, we can derive the magnetic field transport equation (Chandrasekhar, 1961; Pai, 1962; Stuetzer, 1962; Jeffrey, 1966; Lee and Dulikravich, 1991a) as

$$H_{i,t} - \left(v_j H_i - v_i H_j \right)_{,j} = \frac{1}{\mu\sigma} H_{i,jj} \tag{2}$$

Subscripts after the comma designate partial differentiation with respect to the variable or variables that follow the comma. The entire set of Navier-Stokes partial differential equations for the fluid flow and the magnetic transport partial differential equations can be non-dimensionalized by introducing the relations

$$v_i^* = \frac{v_i}{v_o} \qquad x_i^* = \frac{x_i}{l_o} \qquad t^* = \frac{t\, v_o}{l_o} \qquad p^* = \frac{p}{\rho_o v_o^2} \tag{3}$$

$$g^* = \frac{g_i}{g} \qquad H_i^* = \frac{H_i}{H_o} \qquad \theta = \frac{\Delta T}{\Delta T_o} \qquad e^* = \frac{e}{c_{po} \Delta T_o} \tag{4}$$

where T_c is the temperature of the cold wall and T_h is the temperature of the hot wall, so that $\Delta T = T - T_c$, and $\Delta T_o = T_h - T_c$. Here, subscript zero designates reference values, while asterisk designates non-dimensional variables.

In this work only incompressible fluid flow will be considered, while accounting for thermal buoyancy via an extended Boussinesq approximation in the form which is valid even when fluid properties vary as a function of temperature (Gray and Giorgini, 1976). Fluid density and coefficients of specific heat, viscosity and heat conduction can be expressed as general functions of temperature (Gray and Giorgini, 1976)

$$\rho = \rho_o \, \rho'(\theta) \qquad c_p = c_{po} \, c_{po}'(\theta) \tag{5}$$

$$\eta = \eta_o \, \eta'(\theta) \qquad k = k_o \, k'(\theta) \tag{6}$$

where the primed values denote functions of non-dimensional temperature, θ. Here, ρ, η, c_p, and k are fluid density, coefficient of viscosity, coefficient of specific heat at constant pressure, and coefficient of thermal conductivity, respectively. The non-dimensional density ρ' can be expanded in a Taylor series while retaining only the first order term

$$\rho' = 1 - \alpha \, \Delta T = 1 - \alpha^* \, \theta \tag{7}$$

so that

$$\alpha^* = \frac{\partial \rho'}{\partial \theta} = \frac{\Delta T_o \, \rho_o}{\rho_o \, \Delta T_o} \frac{\partial \rho'}{\partial \theta} = \frac{\Delta T_o}{\rho_o} \frac{\partial \rho}{\partial T} = \Delta T_o \, \alpha \tag{8}$$

It can be assumed that the coefficient of thermal expansion, α, is constant in the range of temperatures which are of interest in a particular case. When the term $(\Delta T_o \, \alpha) \ll 1$, equations more general than what is known as Boussinesq approximation can be derived for the fluid with non-constant properties (Gray and Giorgini, 1976). For incompressible flows $c_p = c_v$. Thus, it follows that $de = c_v \, dT = c_p \, dT$. In the case of a liquid/solid mixture the enthalpy per unit mass of the mushy region becomes

$$dh = c_p \, dT + L \, dS \tag{9}$$

where L is the latent heat (enthalpy of solid/liquid phase change) and S is the volumetric fraction of the solid phase. Then

$$v_i \, h_{,i} = c_p \, v_i \, T_{,i} - L \, v_i \, S_{,i} = \left(c_p - L \, S_{,T} \right) v_i \, T_{,i} \tag{10}$$

Let $c_{pe} = c_p - L \, S_{,T}$ be an equivalent specific heat so that

$$c_{pe} = c_{po} \, c_{pe}' = c_{po} \left(c_p' - \frac{L \, S_{,\theta} \, \theta_{,T}}{c_{po}} \right) \tag{11}$$

where S could be an arbitrary function of θ and c_{pe}' is the non-dimensional equivalent specific heat. This approach is called the "enthalpy method" (Poirier and Salcudean, 1986). With the following non-dimensional groups

Reynolds number $\quad Re = \dfrac{\rho_o v_o l_o}{\eta_o}$

Froude number $\quad Fr^2 = \dfrac{v_o^2}{g\, l_o}$

Grashof number $\quad Gr = \dfrac{\rho_o^2\, \alpha\, g\, l_o^3\, \Delta T_o}{\eta_o^2}$

Eckert number $\quad Ec = \dfrac{v_o^2}{c_{po}\, \Delta T_o}$

Prandtl number $\quad Pr = \dfrac{\eta_o\, c_{po}}{k_o}$

Magnetic Prandtl number $\quad Pm = \dfrac{\mu\, \sigma\, \eta_o}{\rho_o}$

Hartmann number $\quad Ht = \mu\, l_o\, H_o \left(\dfrac{\sigma}{\eta_o}\right)^{1/2}$

Magnetic Reynolds number $\quad Rm = Re\, Pm$

Magnetic Mach number $\quad Mm^2 = \dfrac{ReRm}{Ht^2} = \dfrac{\rho_o v_o^2}{\mu\, H_o^2}$ (12)

the conservation laws in non-dimensional form become

$$v_{i,i} = 0 \tag{13}$$

$$v_{i,t} + (v_i\, v_j)_{,j} = \frac{1}{Re}(\eta'\, v_{i,j})_{,j} - \bar{p}_{,i} + \frac{Gr\,\theta}{Re^2}\, g_i + \frac{Ht^2}{RmRe}\,(H_i\, H_k)_{,k} \tag{14}$$

$$\theta_{,t} + v_i\, \theta_{,i} = \frac{1}{RePr\, c_{pe}}(k'\, \theta_{,i})_{,i} + \frac{EcHt^2}{Rm^2 Re\, c_{pe}}\, \varepsilon_{ijk}\varepsilon_{ilm} H_{k,j} H_{m,l} \tag{15}$$

$$H_{,t} - (v_j\, H_i - v_i\, H_j)_{,j} = \frac{1}{Rm}\, H_{i,jj} \tag{16}$$

It should be pointed out that the viscous dissipation can be neglected from an order of magnitude analysis since

$$\frac{\rho_o\, c_{pe}\, \dfrac{\partial T}{\partial t}}{\Phi^{(i)}} = \frac{Re}{Ec} >>> 1 \tag{17}$$

The combination of non-dimensional hydrodynamic, hydrostatic and magnetic pressures is

$$\bar{p} = p + \frac{\phi}{Fr^2} + \frac{1}{Mm^2} H_i H_i \tag{18}$$

where ϕ is the non-dimensional gravity potential defined as $g_i = \phi_{,i}$.

NUMERICAL ALGORITHM

Equations (13-16) represent a global system of coupled non-linear partial differential equations. The global system has been split in two subsystems in order to simplify programming. The Navier-Stokes equations (13-15) constitute the first subsystem and magnetic field transport equations (16) constitute the second subsystem. To integrate each subsystem, the explicit Runge-Kutta time stepping method (Jameson et al., 1981) was used in an alternating manner (Lee and Dulikravich, 1991a).

The general form of each subsystem is the same. The non-dimensional three-dimensional Navier-Stokes equations for incompressible flows in conservative form expressed in generalized curvilinear non-orthogonal coordinates are

$$\frac{\partial \tilde{Q}}{\partial t} + \frac{\partial \tilde{E}}{\partial \xi} + \frac{\partial \tilde{F}}{\partial \eta} + \frac{\partial \tilde{G}}{\partial \zeta} = D^2 + \tilde{S} \tag{19}$$

where $\tilde{Q}$ is the solution vector and $\tilde{E}$, $\tilde{F}$ and $\tilde{G}$ are the flux vectors. The transformed source vector is denoted by $\tilde{S}$. Definitions of these vectors will be given for both systems of equations (Navier-Stokes and magnetic transport) separately. For the Navier-Stokes equations, the generalized vectors are defined as

$$\tilde{Q} = \frac{1}{J}\begin{bmatrix} \bar{p}/\beta \\ u \\ v \\ w \\ \theta \end{bmatrix} \quad \tilde{E} = \frac{1}{J}\begin{bmatrix} U \\ Uu + \xi_x \bar{p} \\ Uv + \xi_y \bar{p} \\ Uw + \xi_z \bar{p} \\ U\theta \end{bmatrix} \quad \tilde{F} = \frac{1}{J}\begin{bmatrix} V \\ Vu + \eta_x \bar{p} \\ Vv + \eta_y \bar{p} \\ Vw + \eta_z \bar{p} \\ V\theta \end{bmatrix}$$

$$\tilde{G} = \frac{1}{J}\begin{bmatrix} W \\ Wu + \zeta_x \bar{p} \\ Wv + \zeta_y \bar{p} \\ Ww + \zeta_z \bar{p} \\ W\theta \end{bmatrix} \quad \tilde{S} = \begin{bmatrix} 0 \\ \tilde{d}_2 \\ \tilde{d}_3 \\ \tilde{d}_4 \\ \tilde{d}_5 \end{bmatrix} \quad \tilde{D} = \frac{1}{Re}\begin{bmatrix} 0 \\ \eta' \\ \eta' \\ \eta' \\ \dfrac{k'}{Pr\, c_p'} \end{bmatrix}^T \tag{20}$$

where $J = \dfrac{\partial(\xi,\eta,\zeta)}{\partial(x,y,z)}$ is the Jacobian determinant of the geometric transformation from physical Cartesian coordinates x, y, z into ξ, η, ζ computational space.

The system of equations given by (13-16) is not hyperbolic since there is no physical time derivative term in the mass conservation equation. Consequently, the system cannot be integrated simultaneously. In order to integrate the system simultaneously and obtain a steady state solution, an artificial compressibility (Chorin, 1967) term, $\dfrac{\partial}{\partial t}\left(\dfrac{\bar{p}}{\beta J}\right)$, has been added to the mass conservation equation (13). Here, β is an artificial compressibility coefficient, a user specified parameter that depends on the problem geometry, grid, flow parameters, etc. (Lee and Dulikravich, 1991c). In the steady state limit the artificial compressibility term tends to zero. Thus, it does not influence the steady state solution.

The source vector $\tilde{S}$ contains the influence of the ponderomotive force due to the magnetic field and the thermal buoyancy force. Its components are given as

$$\tilde{d}_2 = \frac{Ht^2}{RmRe}\left[\frac{\partial}{\partial\xi}\left(\frac{\hat{H}_\xi H_x}{J}\right) + \frac{\partial}{\partial\eta}\left(\frac{\hat{H}_\eta H_y}{J}\right) + \frac{\partial}{\partial\zeta}\left(\frac{\hat{H}_\zeta H_z}{J}\right)\right] + \frac{Gr\theta}{Re^2 J} e_\xi \quad (21)$$

$$\tilde{d}_3 = \frac{Ht^2}{RmRe}\left[\frac{\partial}{\partial\xi}\left(\frac{\hat{H}_\xi H_y}{J}\right) + \frac{\partial}{\partial\eta}\left(\frac{\hat{H}_\eta H_y}{J}\right) + \frac{\partial}{\partial\zeta}\left(\frac{\hat{H}_\zeta H_y}{J}\right)\right] + \frac{Gr\theta}{Re^2 J} e_\eta \quad (22)$$

$$\tilde{d}_4 = \frac{Ht^2}{RmRe}\left[\frac{\partial}{\partial\xi}\left(\frac{\hat{H}_\xi H_z}{J}\right) + \frac{\partial}{\partial\eta}\left(\frac{\hat{H}_\eta H_z}{J}\right) + \frac{\partial}{\partial\zeta}\left(\frac{\hat{H}_\zeta H_z}{J}\right)\right] + \frac{Gr\theta}{Re^2 J} e_\zeta \quad (23)$$

$$\tilde{d}_5 = \frac{1}{c_{pe}} \frac{EcHt^2 J}{RmRe^2}\left[\tilde{P}_1^2 + \tilde{P}_2^2 + \tilde{P}_3^2\right] \quad (24)$$

where H_x, H_y, H_z are the components of the magnetic field vector in Cartesian coordinates, e_ξ e_η, e_ζ are components of the unit vector in the direction of gravity force, and

$$\tilde{P}_1 = \frac{\partial}{\partial\xi}\left(\frac{H_z\xi_y - H_y\xi_z}{J}\right) + \frac{\partial}{\partial\eta}\left(\frac{H_z\eta_y - H_y\eta_z}{J}\right) + \frac{\partial}{\partial\zeta}\left(\frac{H_z\zeta_y - H_y\zeta_z}{J}\right) \quad (25)$$

$$\tilde{P}_2 = \frac{\partial}{\partial\xi}\left(\frac{H_x\xi_z - H_z\xi_x}{J}\right) + \frac{\partial}{\partial\eta}\left(\frac{H_x\eta_z - H_z\eta_x}{J}\right) + \frac{\partial}{\partial\zeta}\left(\frac{H_x\zeta_z - H_z\zeta_x}{J}\right) \quad (26)$$

$$\tilde{P}_3 = \frac{\partial}{\partial\xi}\left(\frac{H_y\xi_x - H_x\xi_y}{J}\right) + \frac{\partial}{\partial\eta}\left(\frac{H_y\eta_x - H_x\eta_y}{J}\right) + \frac{\partial}{\partial\zeta}\left(\frac{H_y\zeta_x - H_x\zeta_y}{J}\right) \quad (27)$$

The diffusion term in general curvilinear coordinates is

$$D^2 = \left(\frac{\tilde{D}}{J} g_{ij}\left(J\tilde{Q}\right)_{,j}\right)_{,i} \quad (28)$$

The metric tensor is defined as

$$g_{ij} = \frac{\partial\bar{x}_i}{\partial\hat{x}_j}\frac{\partial\bar{x}_j}{\partial\hat{x}_i} \quad (29)$$

where $\bar{x}_i$ is the Cartesian coordinate vector and $\hat{x}_i$ is the curvilinear coordinate vector:

$$\bar{x}_i = (x, y, z)^T \qquad \hat{x}_i = (\xi, \eta, \zeta)^T \quad (30)$$

Here, the superscript T represents a transpose. The contravariant components U, V, W of the velocity vector are related to the velocity components u, v, w in the Cartesian system as follows

$$\begin{bmatrix} U \\ V \\ W \end{bmatrix} = \begin{bmatrix} \xi_x & \xi_y & \xi_z \\ \eta_x & \eta_y & \eta_z \\ \zeta_x & \zeta_y & \zeta_z \end{bmatrix} \begin{bmatrix} u \\ v \\ w \end{bmatrix} \quad (31)$$

Similarly, the contravariant components $\hat{H}_\xi$, $\hat{H}_\eta$, $\hat{H}_\zeta$ of the magnetic field vector are defined as

$$\begin{bmatrix} \hat{H}_\xi \\ \hat{H}_\eta \\ \hat{H}_\zeta \end{bmatrix} = \begin{bmatrix} \xi_x & \xi_y & \xi_z \\ \eta_x & \eta_y & \eta_z \\ \zeta_x & \zeta_y & \zeta_z \end{bmatrix} \begin{bmatrix} H_x \\ H_y \\ H_z \end{bmatrix} \quad (32)$$

For the subsystem containing the magnetic field transport equations, the solution vector $\tilde{Q}$, the flux vectors $\tilde{E}$, $\tilde{F}$, $\tilde{G}$, and the source vector $\tilde{S}$ are

$$\tilde{Q} = \frac{1}{J}\begin{bmatrix} H_x \\ H_y \\ H_z \end{bmatrix} \qquad \tilde{E} = \frac{1}{J}\begin{bmatrix} H_xU - u\hat{H}_\xi \\ H_yU - v\hat{H}_\xi \\ H_zU - w\hat{H}_\xi \end{bmatrix} \qquad \tilde{F} = \frac{1}{J}\begin{bmatrix} H_xV - u\hat{H}_\eta \\ H_yV - v\hat{H}_\eta \\ H_zV - w\hat{H}_\eta \end{bmatrix}$$

$$\tilde{G} = \frac{1}{J}\begin{bmatrix} H_xW - u\hat{H}_\zeta \\ H_yW - v\hat{H}_\zeta \\ H_zW - w\hat{H}_\zeta \end{bmatrix} \qquad \tilde{S} = 0 \qquad \tilde{D} = \frac{1}{Rm} I \quad (33)$$

In the case of three-dimensional magnetohydrodynamics, the system of eight partial differential equations needs to be solved by integrating intermittently a subsystem of five fluid flow equations and a subsystem of three magnetic field transport equations and transferring the information through the source-like terms (Lee, 1990; Lee and Dulikravich, 1991a). The explicit Runge-Kutta time-stepping algorithm and finite difference scheme with artificial compressibility (Chorin, 1967) were used in the general non-orthogonal curvilinear boundary conforming coordinate system. The explicit time integration scheme was used because it can be efficiently vectorized and because additional equations can be easily added to the system. The rate of convergence of explicit schemes is generally much lower than for implicit schemes, but when fully vectorized, these schemes need less central processor unit time to reach convergence than implicit schemes. This advantage of explicit schemes is more pronounced when three-dimensional problems with complex geometries are studied.

COMPUTATIONAL RESULTS

A computer code written in Fortran was developed for simulation of two-dimensional solidification processes under the influence of a steady externally applied magnetic field. Three configurations were tested numerically: a closed container cooled uniformly from above, a straight channel flow with non-uniformly cooled top and bottom walls, and a U-shaped channel with non-uniformly cooled inner and outer walls. Non-dimensional parameters used in the calculations are summarized in Table 1.

Passage	Closed	Straight	U-shaped	Arbitrary
Melt	(silicon)	(undefined)	(undefined)	(saline)
Gr	56.769×10^6	0.0	0.0	0.0
Re	8300	100	20	234.44
Ec	7.869×10^{-8}	1	1	6.46×10^{-8}
Pr	0.0116	7.9	7.9	36.9
Pm	4.44×10^{-6}	1	1	2.68×10^{-3}
Ht	$209.3B_o$ or $2093\ B_o$	5 or 10	5 or 10	0.0 or $0.5027\ B_o$

TABLE 1. Nondimensional Numbers

Closed Container

Mathematical and numerical models for solidification of a fluid flow were first tested in the case of a closed rectangular container of aspect ratio 3:1. It was discretized with 60x60 grid cells that were clustered towards the four walls. Vertical walls were thermally insulated, while the top wall had a uniform undercooling non-dimensional temperature of $\theta = -10$. At the same time, the bottom wall had a uniform non-dimensional temperature of $\theta = 1$. A uniform magnetic field of $Ht = 209.3\ B_0$ was applied vertically downward. We have specified $B_0 = 1$ Tesla. The resulting velocity vector field (Fig. 1a) indicates strong recirculation of the melt due to thermal buoyancy. The solid accrued is visible towards the top wall. The resulting magnetic force lines (lines that are locally tangent to the magnetic force) are depicted in Fig. 1b indicating that the fluid motion has distorted the magnetic force lines.

When a stronger magnetic field ($Ht = 2093\ B_0$) was applied, the thermal buoyancy flow was significantly suppressed (Fig. 2a) and the magnetic force lines straightened somewhat (Fig. 2b). The amount of solid accrued at the top wall is smaller than with $Ht = 209.3\ B_0$.

Straight Channel

The second configuration studied was a straight two-dimensional channel of aspect ratio 3:1 with the flow direction from left to right (Fig.3a). A uniform non-dimensional temperature $\theta = 1$ was imposed at the inlet. Along the walls a smoothly varying cooling was specified as $\theta = 1 - 11 \sin(\pi x/3)$. Both velocity components were specified at the inlet, while combination of hydrostatic, hydromagnetic and hydrodynamic pressure was specified at the exit. Properties of the fluid flow were defined by the non-dimensional numbers which are given in Table 1. All physical properties were assumed not to vary with temperature. The flow field was discretized with 60×60 non-clustered grid cells.

The first test case represents a solidifying flow field with an imposed uniform magnetic field of $Ht = 5$ acting vertically downward. The computed velocity vector field clearly outlines the solidified zones attached to the channel walls as given in Fig. 3a. Computed lines of magnetic force are given in Fig. 3b indicating that they have been strongly affected by the flow field.

To test the influence of a stronger magnetic field on solidification, a test run was performed with the viscosity varying linearly in the mushy region and a vertically downward pointing constant magnetic field of $Ht = 10$. The computed velocity vector field (Fig. 4a) and the magnetic lines of force (Fig. 4b) demonstrate that the magnetic field is affected even further by the flow field. The presence of a magnetic field inhibits the growth of the solid layers because of the higher speed of the fluid next to the solid/fluid interface. This is typical for magnetohydrodynamics.

U-shaped Channel

The next test configuration represented a solidifying flow in a U-shaped channel of constant width where the fluid enters at the upper end and exits at the lower end. The same type of boundary conditions was imposed on inlet temperature and velocity as in the case of a straight channel. Along the straight parts of the walls the temperature was kept constant ($\theta = 1$). Along the curved parts of the walls the non-dimensional temperature varied according to $\theta = 1 - 11 \sin(\pi/2 - \omega)$ where ω is the angle between the wall point and the horizontal. The computational grid had 264×60 cells that were clustered towards the walls. Non-dimensional numbers used with the U-shaped channel are given in Table 1.

In the first test case a uniform magnetic field ($Ht = 5$) was applied perpendicular to the walls of the entire U-shaped channel. The computed velocity vector field (Fig. 5a) demonstrate that the magnetic field effectively eliminates flow recirculation regions. The predicted magnetic force lines (Fig. 5b) are significantly distorted from the straight-line pattern that would connect inner and outer walls if there would be no flow through the channel.

In the second test case a stronger magnetic field ($Ht = 10$) was applied in the same manner resulting in a dramatic change in the flow pattern (Fig. 6a). Plot of the magnetic lines of force (Fig. 6b) demonstrate their complex pattern that could be exploited to position and orient short feromagnetically coated fibers in the flow field and, consequently, in the solidified layers.

In the case that the externally applied magnetic field is not uniform, but instead varies along the curved parts of the channel walls according to $Ht = 10 - 5 \sin(\pi/2 - \omega)$, the flow field pattern (Fig. 7a) and the magnetic lines of force (Fig. 7b) will be considerably different. This clearly demonstrates the conceptual feasibility of controlling not only the orientation but also the concentration of the fibers in the resin during the curing process.

Arbitrary Channel

Finally, the mathematical model and the computer code were tested using a set of physical flow parameters corresponding to a saline solution flow in an arbitrary shaped channel with undercooled walls. As in the case of channel flow, the temperature of the walls from inlet to exit was varying according to a sinusoidal distribution $\theta = 1 - 11 \sin(\pi\, i / imax)$ where i is the grid cell index in the x-direction ($1 < i < imax$). Fluid temperature at the inlet was a uniform $T = 283$ K corresponding to $\theta = 1$ since $T_h = 283$ K and $T_c = 273$ K so that $\Delta T_o = T_h - T_c = 10$ K. This made the coldest point on the wall have a temperature of -100 degrees Celsius. In the case when a steady uniform magnetic field was applied, it acted vertically downward between the inlet and 80% of the channel length, while no magnetic field was applied over the remaining 20% of the channel length. The characteristic quantities that were used for non-dimensionalization are: $c_{po} = c_{po\ liq}$, $k_o = k_{o\ liq}$, $l_o = 0.01$ m, $v_o = 0.1$ m/s. Since the value for the magnetic permeability could not be found in the open literature, we have arbitrarily assumed it to be $\mu = 50\ \mu_v$, where $\mu_v = 4\pi \times 10^{-7}$ is the magnetic permeability for vacuum. If $B_0 = \mu_v H_0$, the remaining terms in the equation for Ht can be grouped so that Ht is directly proportional to B_0 which is measured in Teslas. For example, if $Ht = 0.5\ B_0$ and the value for B_0 is 10, this means that the Hartmann number $Ht = 5$ can be achieved with the magnetic field of 10 T.

The non-orthogonal boundary-conforming computational grid consisted of 100x58 grid cells that were clustered towards the inlet and the passage top and bottom walls. The grid was generated using our grid optimization algorithm (Kennon and Dulikravich, 1986).

A comparison of the computational results with and without an external magnetic field shows that the velocity profiles change under the influence of the magnetic field due to the ponderomotive force (Figs. 8a and 9a). More importantly, the solidified layers in the case where no external magnetic field was applied are thicker and differently shaped compared to the freezing with the magnetic field as indicated by the isotherms in the solid phase without (Fig. 8b) and with (Fig. 9b) the magnetic field. A very complex pattern of magnetic lines of force (Fig. 10a) clearly indicates that the coated short fibers could be manipulated using appropriately distributed magnetic field strength along the boundaries of the domain. It should be pointed out that it is the higher speed of the fluid close to the solid/liquid interface that decreases the residence time of the fluid particles in the mushy region, thus decreasing the rate of solid accretion. This increase in the fluid speed in the boundary layer regions is caused by the presence of the magnetic field. On the other hand, Joule heating (Fig. 10b) would have a profound influence on the solidification rate in the case of a lower electrical conductivity of the fluid and in flows generated purely by thermal buoyancy

CONCLUSIONS

A complete analytical and numerical formulation has been developed for the theoretical prediction of solidification processes in fluid flows inside undercooled passages with and without the influence of an externally applied steady magnetic field. Computational results confirm that the magnetic field has a profound

influence on the solidifying flow field since it eliminates flow recirculation regions and causes distorted velocity profiles having pronounced overshoots close to the solid boundaries. Temperature field also changes under the influence of the external magnetic field. This change influences heat transfer through the boundaries and consequently the amount of the solid phase accrued on undercooled walls. Specifically, the influence of the ponderomotive force and, to a much lesser extent, Joule heating are such that they tend to reduce the amount of the accrued solid phase. Combined with the predicted complex patterns of the magnetic field force lines, this indicates a possibility for the development of a computational optimization algorithm capable of achieving desired configurations of the solidifyed layers and desired distribution and orientation of magnetised short fibers within the solidifyed layers.

ACKNOWLEDGMENTS

All computations were performed remotely on the Cray-YMP computer at NASA Ames Research Center NAS facility and at Cray Research, Inc. in Eagan, Minnesota and post processed at Penn State on equipment donated by Apple Computer, Inc. Authors are thankful to Mr. Scott G. Sheffer for correcting the grammar in this paper.

REFERENCES

Balasubramaniam, T.A. and Bowman, H.F., 1977, "Thermal Conductivity and Thermal Diffusivity of Biomaterials: A Simultaneous Measurement Technique," *Journal of Biomed. Eng.* August, pp. 148-154.

Cranston, J.J. and Reitz, J.A.III, 1980, "SMC Molding Techniques for Optimized Mechanical Properties in Structural Applications," *Polymer and Plastics Technology and Engineering*, Vol. 15, pp. 97-114.

Chandrasekhar, S., 1961, "Hydrodynamic and Hydromagnetic Stability," Dover Publication Inc., New York.

Chorin, A. J., 1967, "A Numerical Method for Solving Incompressible Viscous Flow Problems," *Journal of Computational Physics*, Vol. 2, pp. 12-26.

Diller, K. R., 1985, "The Influence of Controlled Ice Nucleation on Regulating the Thermal History During Freezing," *Cryobiology*, Vol. 22, pp. 268-281.

Dulikravich, G. S. and Hayes, L. J., 1988, "Control of Surface Temperatures to Optimize Survival in Cryopreservation," Proc. of ASME WAM '88 *Symposium on Computational Methods in Bioengineering*, ed. R. L. Spilker and B. R. Simon, Chicago, IL, Nov. 27-Dec.2, BED-9, pp. 255-265.

Dulikravich, G.S. and Kosovic, B, 1992, "Solidification of Variable Property Melts Under the Influence of Low Gravity, Magnetic Fields and Electric Fields," AIAA paper 92-0694, AIAA Aerospace Sciences Meeting, Reno, NV, Jan. 6-9.

Lee, S. and Dulikravich, G. S., 1991b, "Computation of Magnetohydrodynamic Flow With Joule Heating and Buoyancy," *Proc. of Internati. Aerospace Congress*, Melbourne, Australia, May.

Lee, S. and Dulikravich, G.S., 1991c, "Performance Analysis of DMR Method for Acceleration of Iterative Algorithms," AIAA paper 91-0241, AIAA Aerospace Sciences Meeting, Reno, NV, January 7-10.

Lee, S., Dulikravich, G. S. and Kosovic, B., 1991a, "Interaction of a Magnetic Field with Blood Flow," Proc. 17th Annual Northeast Bioengineering Conference, Univ. of Connecticut, Hartford, CT, April 4-5.

Lee, S., Dulikravich, G. S. and Kosovic, B., 1991b, "Electrohydrodynamic (EHD) Flow Modeling and Computations," AIAA paper 91-1469, AIAA Plasma Physics, Fluid Dynamics and Lasers Conference, Honolulu, Hawaii, June 24-26.

Ozoe, H. and Okada, K. , 1989, "The Effect of the Direction of the External Magnetic Field on the Three-Dimensional Natural Convection in a Cubical Enclosure," *International Journal of Heat and Mass Transfer*, Vol. 32, No. 2, pp. 1939-1954.

Pai, S.-I. , 1962, "Magnetogasdynamics and Plasma Dynamics," Springer Verlag, Vienna.

Poirier, D. and Salcudean, M., 1986, "On Numerical Methods Used in Mathematical Modeling of Phase Change in Liquid Metals", ASME paper 86-WAM/HT-22, Anaheim, CA, Dec. 7-12.

Stuetzer, O. M., 1962, "Magnetohydrodynamics and Electrohydrodynamics," *The Physics of Fluids*, Vol. 5, No. 5, pp. 534-544.

Sud,V.K., Sekhon, G.S. and Mishra, R.K., 1977, "Pumping Action of Blood by a Magnetic Field," *Bulletin of Mathematical Biology*, Vol. 39, pp.385-390.

Vives, C., 1989, "Effects of a Magnetically Forced Convection During the Crystallization in Mould of Aluminum Alloys," *Journal of Crystal Growth*, Vol. 94, pp. 739-750.

Yamashita, S., Hatta, H., Sugano, T. and Murayama, K., 1989, "Fiber Orientation Control of Short Fiber Composites: Experiment," *Journal of Composite Materials*, Vol. 23, pp. 32-41.

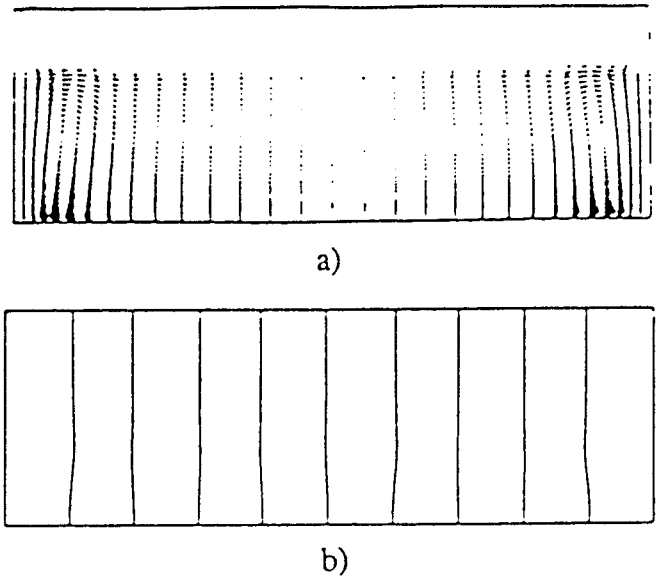

Fig. 1. Closed Container With a Weak Constant Magnetic Field
a) velocity vector field; b) magnetic lines of force

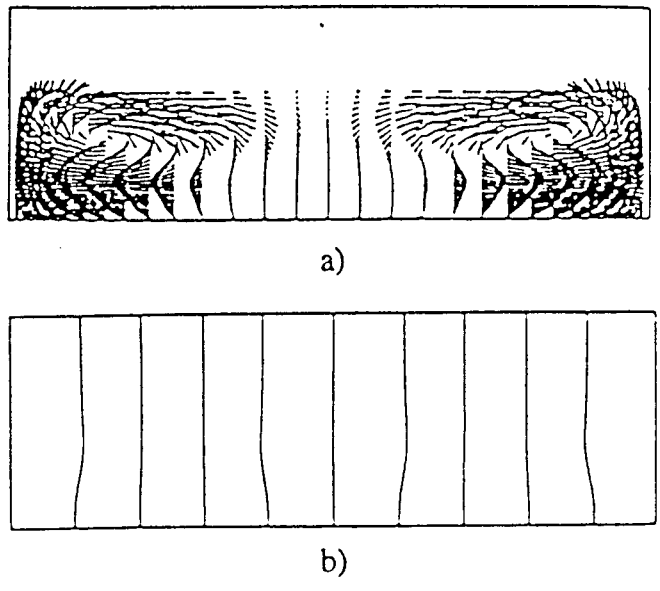

Fig. 2. Closed Container With a Strong Constant Magnetic Field
a) velocity vector field; b) magnetic lines of force

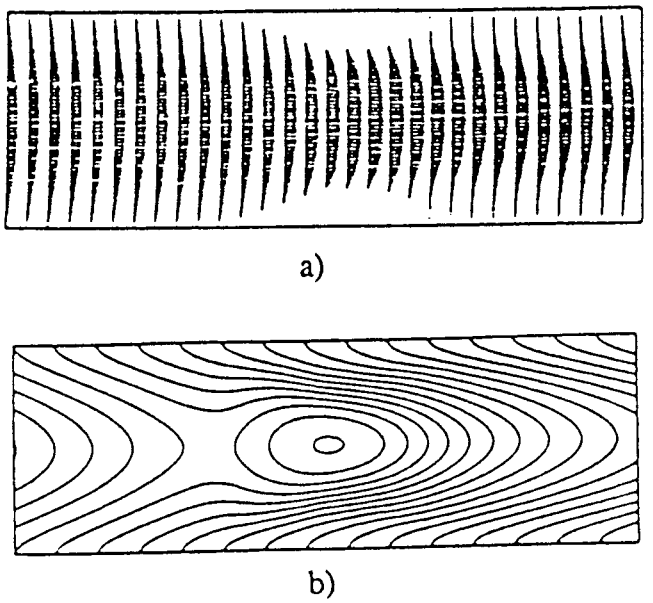

Fig. 3. Straight Channel With a Weak Constant Magnetic Field
a) velocity vector field; b) magnetic lines of force

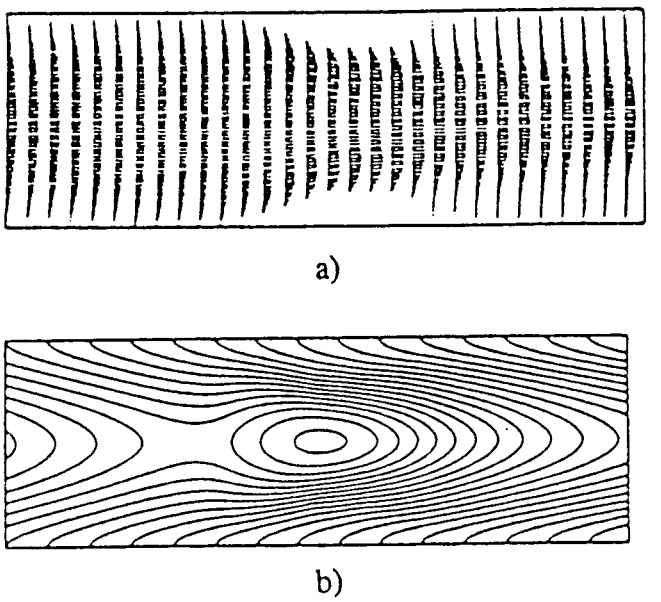

Fig. 4. Straight Channel With a Strong Constant Magnetic Field
a) velocity vector field; b) magnetic lines of force

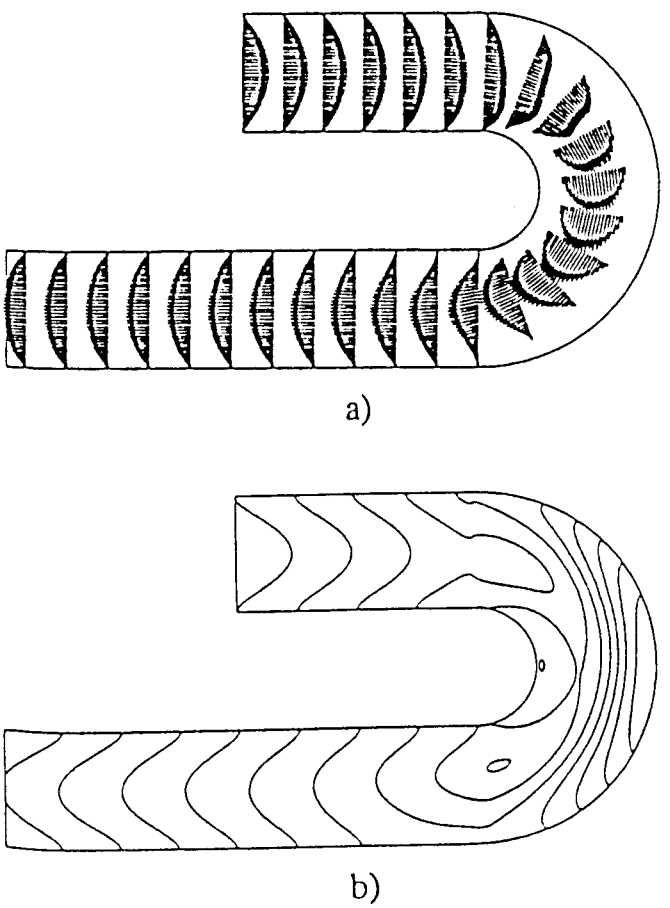

Fig. 5. U-shaped Channel With a Weak Constant Magnetic Field
a) velocity vector field; b) magnetic lines of force

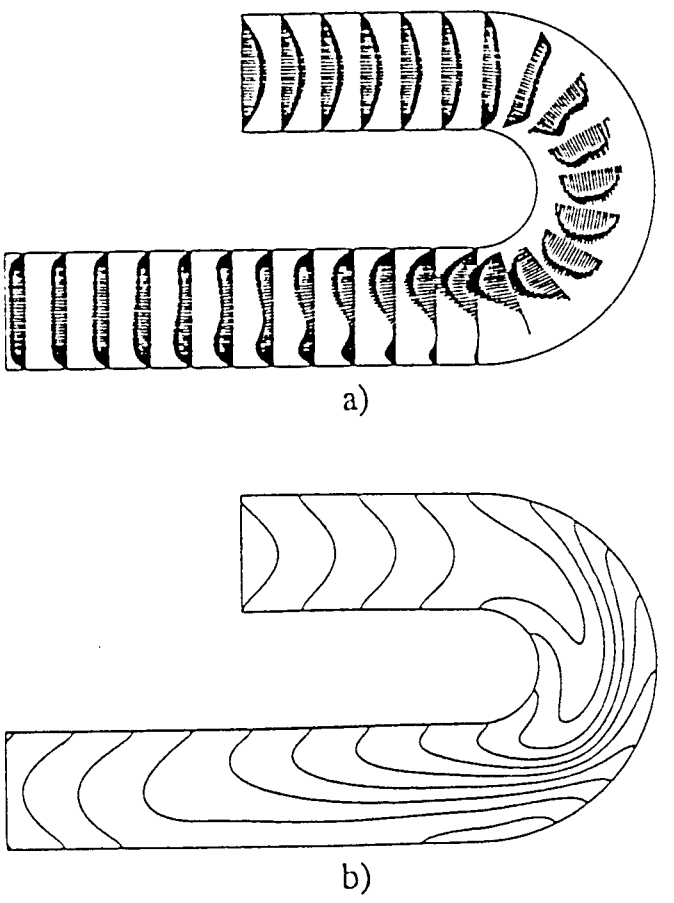

Fig. 6. U-shaped Channel With a Strong Constant Magnetic Field
a) velocity vector field; b) magnetic lines of force

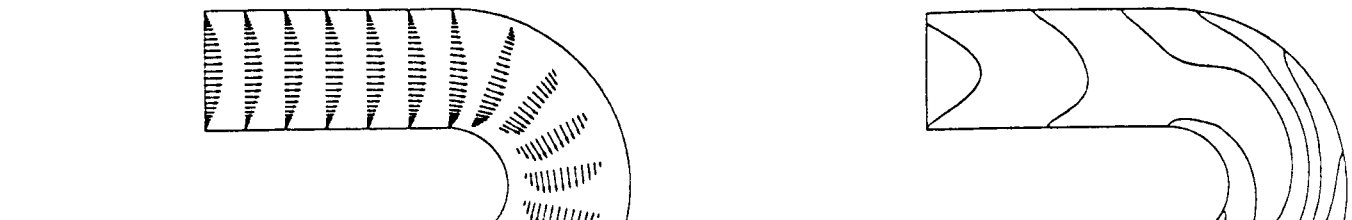

Fig. 7. U-shaped Channel With a Variable Magnetic Field
a) velocity vector field; b) magnetic lines of force

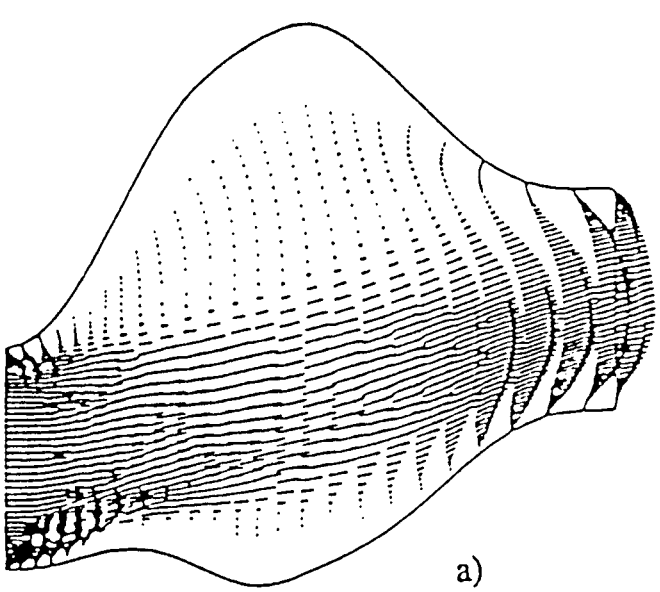

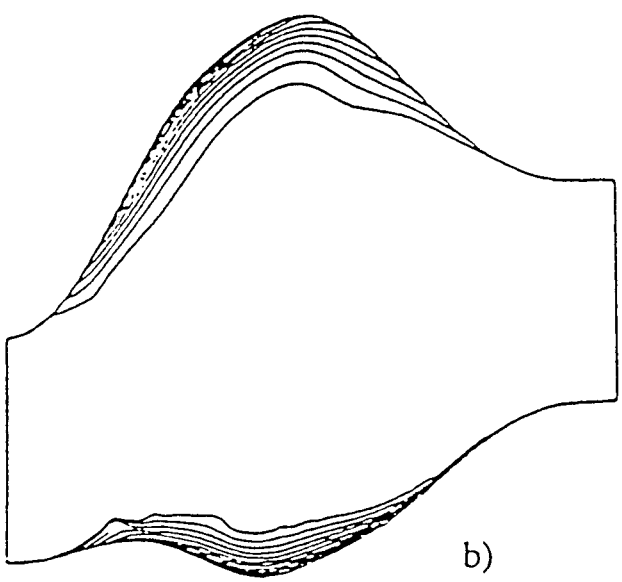

Fig. 8. Arbitrary Passage Without Magnetic Field
a) velocity vector field; b) isotherms

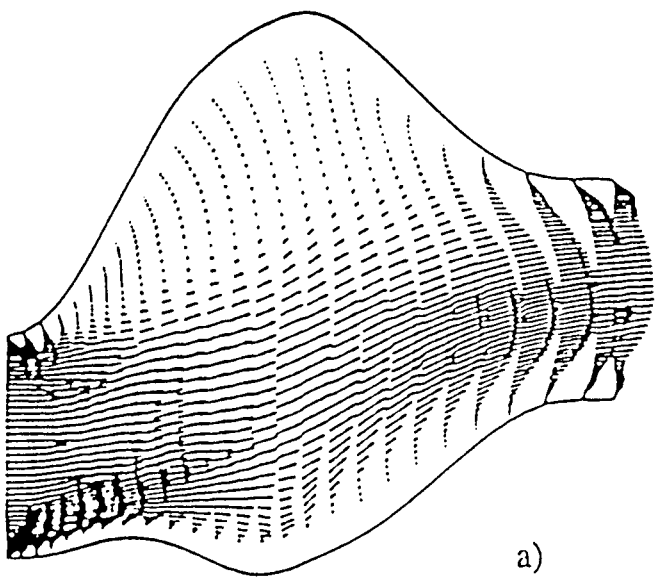

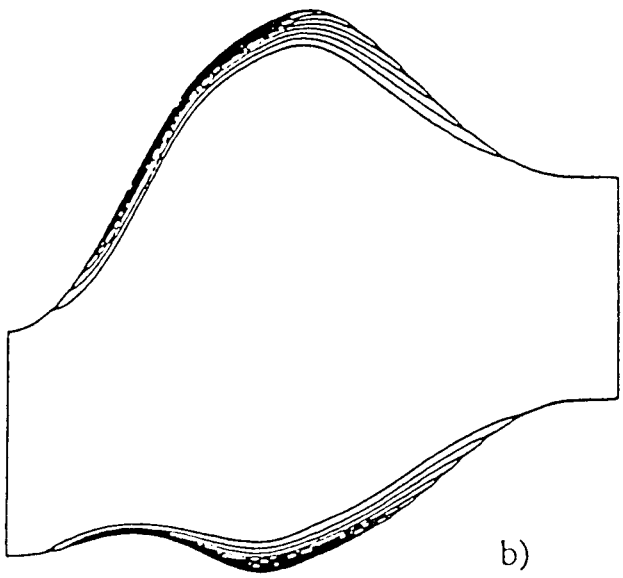

Fig. 9. Arbitrary Passage With a Constant Magnetic Field
a) velocity vector field; b) isotherms

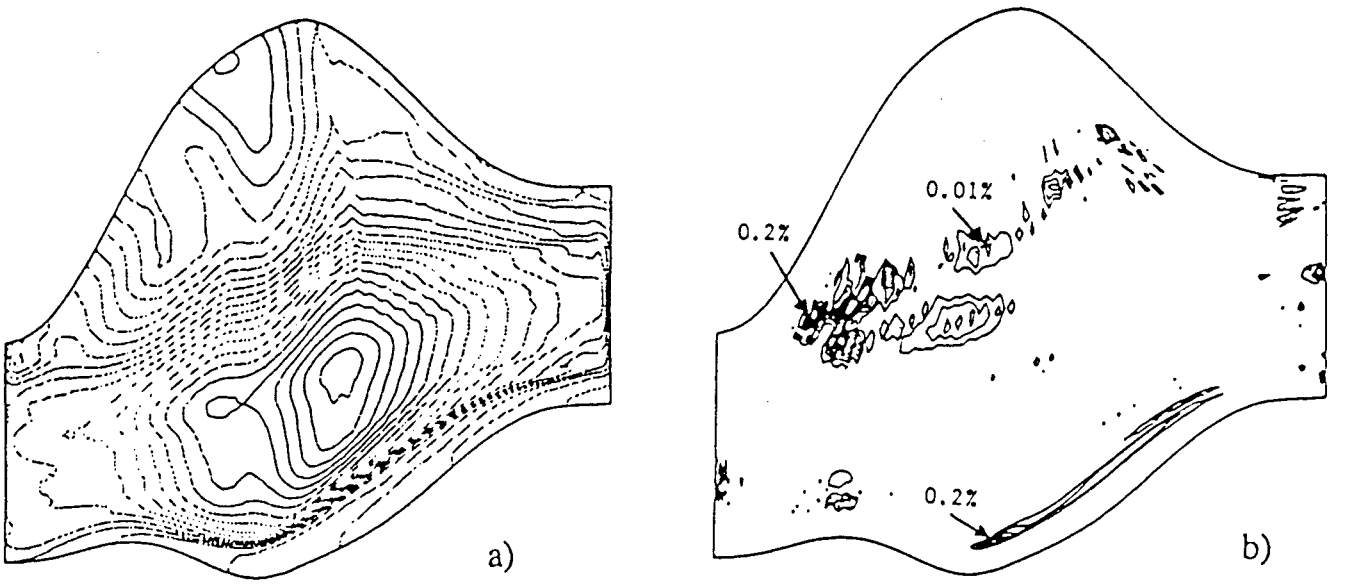

Fig. 10. Arbitrary Passage With a Constant Magnetic Field
a) magnetic lines of force; b) Joule heating contours